Heliyon 7 (2021) e06247

Contents lists available at ScienceDirect

Heliyon

journal homepage: www.cell.com/heliyon

Research article

Compact hexa-band bio-inspired antenna using asymmetric microstrip feeding technique for wireless applications

Jeremiah O. Abolade [a,*], Dominic B.O. Konditi [b], Vasant.M. Dharmadhikary [c]

[a] Department of Electrical Engineering, Pan African University, Institute for Basic Sciences, Technology and Innovation, Nairobi, Kenya
[b] School of Electrical and Electronic Engineering, The Technical University of Kenya, Nairobi, Kenya
[c] Department of Electrical and Electronic Engineering, Dedan Kimathi University of Technology, Nyeri, Kenya

ARTICLE INFO

Keywords:
Compact multiband antenna
Bio-inspired antenna
Asymmetric microstrip feedline (AMF)
Fifth generation (5G)
Hexa-band antenna
Vitis vinifera

ABSTRACT

A compact Hexa-band Bio-inspired antenna is presented in this paper. The structure of the proposed antenna is realized from a semi-Vine-leaf shape, Defected Ground Structure (DGS) and arc-slots techniques. The total dimension of the antenna is 0.35λd x 0.14λd; where λd is the guided wavelength at low frequency (2.37GHz). The design begins with a semi-*Vitis vinifera* leaf-shaped radiating patch monopole structure, fed with an asymmetric microstrip feedline to achieve compactness. Five (5) arc slits are then introduced on the radiating patch of the initiator with an intention to create band notches and thereby results in multiband and further miniaturization. The proposed antenna is analyzed, simulated and fabricated. The measurement results of the proposed antenna show that the antenna operates at 2.37GHz, 3.06GHz, 3.52GHz, 4.28GHz, 4.88GHz, and 6.0GHz with a -10dB fractional bandwidth of 11.97%, 4.61%, 12.43%, 6.77%, 2.46%, and 11.55% respectively. The peak gain of the proposed antenna is 3.21 dBi. The radiation patterns of the proposed antenna are Bi-directional at XZ-plane and XY-plane, but Omnidirectional at YZ-plane. Owing to the compactness of the antenna, suitable radiation pattern, acceptable gain and high radiation efficiency, the proposed antenna is suitable for several applications such as Industrial, Scientific and Medical (ISM) Band, Radar, WiMAX, 5G mid-band, Bluetooth, WLAN, WiMAX, LTE, and Wi-Fi. The contributions of this work are: (i) the use of asymmetric microstrip feedline for miniaturization purpose contrary to the commonly used asymmetric coplanar strip; (ii) simple formulation for the predictions of notch bands introduced by the slit on the radiating patch; and (iii) presentation of ultra-compact hexa-band antenna compared to the existing multiband antenna.

1. Introduction

Wireless communication has evolved over the years with several bands in different nations of the world. This has necessitated the need for multiband antennas. Antenna, being the backbone of wireless communication, determines the size of such devices. Nowadays, Antennas with compact-size, multiband accompany with suitable gain and radiation pattern are on ever increasing demand in wireless communication markets.

Over the years, the attention of researchers has been directed in this direction and the majority of the works in the literature have concentrated on multiband antennas for WLAN, WiMAX and ISM band applications [1, 2, 3, 4, 5, 6, 7, 8, 9, 10, 11, 12, 13, 14, 15, 16, 17, 18]. Nonetheless, with the recent deployment of 5G technology, it is necessary to incorporate some of its proposed operating frequency bands with other existing bands while ensuring compactness.

In achieving multiband antenna, slot etching on the ground plane or on the radiating patch has been used in the literature to achieve multi-frequency resonances [1, 2, 4, 5, 10, 19]. Metamaterial has also been used for multiband antennas realization as reported by authors in [3, 16]. Furthermore, the authors in [12], and [14] have used electromagnetic Band Gap (EBG) and meandering to realize compact multiband antennas. Parasitic loading has also been used by authors in [20] for multiband antenna realization. One of the advantages of patch antennas is the availability of different feeding techniques such as coaxial, microstrip, coplanar waveguide (CPW).

* Corresponding author.
E-mail address: aboladejeremiah@yahoo.com (J.O. Abolade).

https://doi.org/10.1016/j.heliyon.2021.e06247
Received 12 January 2021; Received in revised form 1 February 2021; Accepted 5 February 2021

Figure 1. A typical Vine-leaf.

Coplanar waveguide can be divided into symmetrical and Asymmetrical coplanar waveguide. Due to the benefits presented by CPW such as small radiation leakage, less dispersion, the independence of its characteristic impedance on the thickness of the substrate, uniplanar and ease of integration with other microwave devices, it has been popularly employed as the feeding techniques of patch antennas. For symmetrical CPW, the strip is situated at the center of the two ground planes [6, 7, 8, 9, 17, 18, 21]. On the other hand, Asymmetric CPW usually referred to as asymmetric coplanar strip (ACS) has a strip shifted from the center of the ground plane and usually has its ground plane on one side of the strip [15, 22]. ACS, along with the benefit of CPW, gives a high degree of freedom to achieve compact structure. In this work, an Asymmetric microstrip fed antenna is proposed.

The contributions of this work are as follows: (i) the use of asymmetric microstrip feedline for miniaturization purpose contrary to the commonly used asymmetric coplanar strip; (ii) simple formulation for the predictions of notch bands introduced by the slit on the radiating patch; and (iii) presentation of ultra-compact hexa-band antenna compared to the existing multiband antennas.

2. Antenna design and analysis

The Bio-inspired asymmetric microstrip fed antenna (BioAs-MPAs) proposed in this work is based on a Semi-Vine-leaf radiating patch structure with an asymmetric microstrip feedline. A typical Vine-leaf is as shown in Figure 1. The motivation behind the choice of Vine-leaf is due to the saw-toothlike shape of its edge which increases the perimeter of the structure. The evolution of the proposed structure is presented in Figure 2 and the optimized design parameters are presented in Table 1.

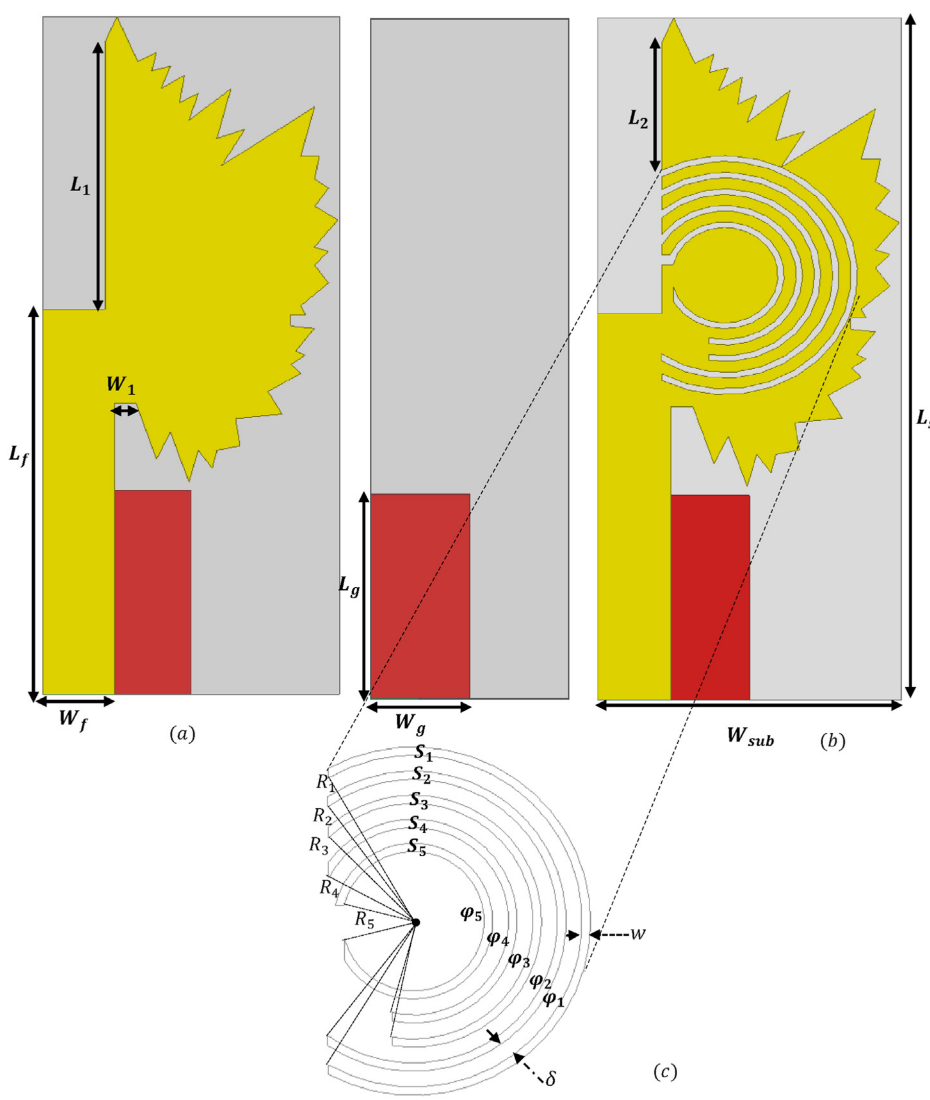

Figure 2. The configuration of (a) design Initiator (b) Proposed antenna (c) The embedded arc-slot.

Table 1. The optimized design parameters of the proposed structure.

Parameter	W_{sub}	W_g	W_f	W_1	L_{sub}
Value (mm)	12	6	2.9	0.9	30
Parameter	L_g	L_f	L_1	L_2	
Value (mm)	9	17	11.9	5.6	

Table 2. The coordinates of the Semi-Vine-leaf-shape used as the radiating patch.

Semi-Vine-leaf co-ordinate points								
n	X	Y	n	X	Y	n	X	Y
1	9.6	-1.6	**16**	3.6	-6.1	**31**	-3.4	-4.2
2	8.4	-2.2	**17**	3.2	-6.5	**32**	-5.0	-5.2
3	10.6	-2.9	**18**	3.2	-7.6	**33**	-4.6	-4.0
4	9.2	-3.3	**19**	2.8	-7.4	**34**	-6.8	-4.6
5	10.0	-3.9	**20**	1.8	-8.6	**35**	-5.4	-2.9
6	9.2	-4.0	**21**	1.0	-8.0	**36**	-6.6	-3.3
7	9.0	-5.0	**22**	0.4	-8.6	**37**	-6.2	-2.5
8	7.8	-4.8	**23**	0.2	-8.0	**38**	-7.4	-2.7
9	7.6	-6.7	**24**	-1.0	-8.9	**39**	-6.8	-1.8
10	6.6	-6.1	**25**	-1.6	-8.0	**40**	-7.8	-2.2
11	5.8	-7.4	**26**	-2.4	-8.6	**41**	-7.6	-1.4
12	5.4	-7.0	**27**	-2.8	-8.0	**42**	-8.4	-1.6
13	5.0	-7.6	**28**	-3.8	-8.2	**43**	-8.0	-0.8
14	4.8	-7.2	**29**	-3.8	-7.4	**44**	-10.0	0.0
15	3.8	-8.0	**30**	-6.0	-8.0	**45**	-8.9	0.4
						46	4.8	0.5

The values of parameters in Table 1 are derived from the parametric study of the proposed structure. First, we start with an unslotted semi-Vine-leaf shape having a total perimeter (ψ) of 70.5mm on a Duroid 5880 substrate with a thickness of 1.57mm as shown in Figure 2a. The perimeter of the proposed radiating patch is determined from its co-ordinates by using Eq. (1). The coordinate of the proposed patch is given in Table 2. The resonance of the proposed structure can be predicted by using Eq. (2) [23]. Secondly, arc-slots (S1, S2, S3, S4 and S5) are introduced as shown in Figure 2b. The arc-slots are carefully designed by employing quarter wavelength strips. The design of the arc strip is done using Eqs. (4), (5), (6), (7), (8), (9), (10), and (11) and the optimized arc-slot design parameters with the resonant frequency of the respective strips are presented in Table 3.where; N = 46 from Table 2 and

$$\psi = \sum_{n=1}^{N-1}\left[\sqrt{(x_{n+1}-x_n)^2+(y_{n+1}-y_n)^2}\right] \tag{1}$$

$$f_r \approx \frac{300}{\psi\sqrt{\varepsilon_{reff}}} \tag{2}$$

$$\varepsilon_{reff} \approx \frac{\varepsilon_r+1}{2} \tag{3}$$

ψ is the perimeter of the patch, ε_{reff} is the effective relative permittivity, According to the theory of strip line [24], the strip used for slitting in this work is formulated as follows:

$$l_i = \frac{\lambda_i}{4} \tag{4}$$

$$\lambda_i = \frac{c_o}{f_i} \tag{5}$$

Where, l_i is the length of the ith strip, λ_i is the free space wavelength of ith strip, and f_i is the resonance frequency of the ith strip in air. Considering the permittivity of the dielectric, the resonance frequency of ith strip becomes

$$f_i = \frac{c_o}{\lambda_{di}} \tag{6}$$

Where λ_{di} is the wavelength in the dielectric of the ith strip and it is defined as;

Table 3. The optimized parameter of the Arc-shape strip and the respective resonance frequency.

Arc-Strip (S)	R_1 (mm)	r_1 (mm)	ϕ_i(^{o})	δ (mm)	g_i (mm)	l_i (mm)	f_r (GHz)
S_1	5.000	5.250	236.57	0.286	11.30	21.70	2.735
S_2	4.275	4.525	247.51	0.306	8.90	19.50	3.033
S_3	3.550	3.800	230.66	0.253	8.60	15.30	3.875
S_4	2.825	3.075	246.11	0.256	6.10	13.20	4.488
S_5	2.100	2.350	306.68	0.256	2.20	12.60	4.713

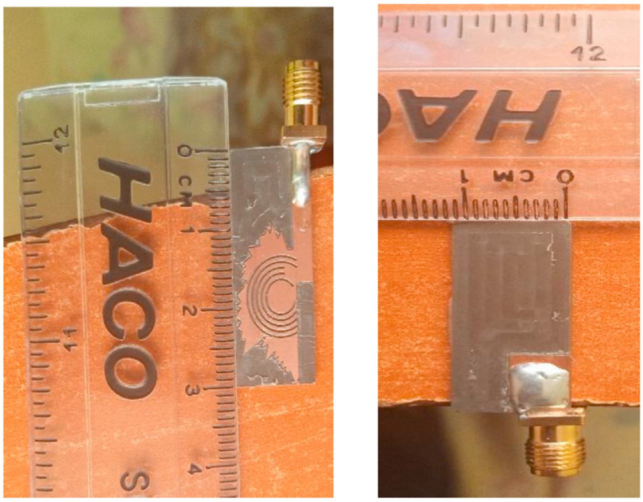

(a) (b)

Figure 3. (a) Top view of the prototype, (b)bottom view of the prototype of the proposed antenna.

$$\lambda_{di} = \frac{\lambda_i}{\sqrt{\varepsilon_r}} \tag{7}$$

Hence,

$$f_i = \frac{c_o}{4l_i\sqrt{\varepsilon_{reff}}} \tag{8}$$

Where ε_{eff} replaces ε_r to incorporate the fringe effect and it is defined as given in Eq. (3)

$$l_i = 2\pi r_i - g_i \tag{9}$$

$$g_i = \frac{(\theta - \varphi_i)\text{x}2\pi r_i}{\theta} \tag{10}$$

$$r_i = R_i + w \tag{11}$$

where; r_i is the external radius of the ith strip, R_i is the internal radius of the ith strip, w is the width of the strip (0.25mm), g_i is the slot-length of the ith strip, θ is the angle of a circle (i.e., 360°), and ϕ_i is the angle subtended by an ith strip. δ is the width of the parallel wires gap as depicted in Figure 2c.

Therefore, the arc-slots S_1, S_2, S_3, S_4, *and* S_5 are expected to produce band notches at 2.73GHz, 3.03GHz, 3.88GHz, 4.49GHz and 4.71GHz respectively. Hence, the realization of the realization of the multiband antenna. The proposed antenna is fed with a 50Ω feedline. The top view and the bottom layer of the fabricated proposed antenna are as shown in Fig. 3a and b respectively.

3. Result and discussion

In this section, the reflection coefficient, Radiation pattern, surface current distribution, gain and efficiency are presented.

3.1. Reflection coefficient (S_{11})

Figure 4a shows the reflection coefficient of the evolution of the proposed structure. It can be observed from Figure 4a that the initiator (Figure 2a) has two resonance frequencies at 3.86GHz and 7.32GHz with a S11 of -35dB and -13dB; a fractional bandwidth of 44.8% and 14.7% respectively. The introduction of the Arc-slot S_1 (Ant. 1) results in the band notch at 2.7GHz, which validates the analytical design and eventually results in resonance at 2.46GHz, 4.3GHz, and 6.74GHz with a S11 of -16.01dB, -24.46dB, and -51.68dB; a fractional bandwidth of 1.2%, 40.9%, and 13.8% respectively.

With the arc-slot S_2 (Ant. 2), a band notch is observed at 3.06GHz and results in resonance at 2.74GHz, 4.4GHz and 7.1GHz with a S11 of -17.1dB, 21.9dB and -18.3dB; a fractional bandwidth of 2.2%, 43.0%, and 15.7% respectively. Similarly, the arc-slot S_3 (Ant. 3) produces a band notch at 3.9GHz as predicted earlier and results in a dual band antenna with resonance at 3.15GHz and 5.2GHz with a S11 of -35.2dB, and -21.3dB; a fractional bandwidth of 6.7% and 57.3% respectively.

In the same light, the arc-slot S_4 (Ant. 4) gives a band notch at 4.48GHz as predicted in Table 3 which results in a dual band antenna operating at 3.36GHz and 5.6GHz with a S11 of -43.63dB and -23.27dB; a fractional bandwidth of 11.0% and 41.0% respectively. Finally, arc-slot S_5 (Ant. 5) gives a notch band at 4.7GHz as seen in Figure 4a and it results in dual band antenna with resonances at 3.47GHz and 5.58GHz with a S11 of -34.2dB and -26.1dB; a fractional bandwidth of 13.8% and 45.1% respectively. Therefore, each of the proposed arc slots results in multi-resonance with a good return loss (RL).

Consequently, all the arc-slots are then combined to achieve a robust multiband antenna as seen in Figure 4a. The addition of all the arc-slits results in Hexa-band antenna while maintaining the notches as predicted in section II. It can be seen in Figure 4b that there is no significant difference between the measurement and the simulation results. Hence,

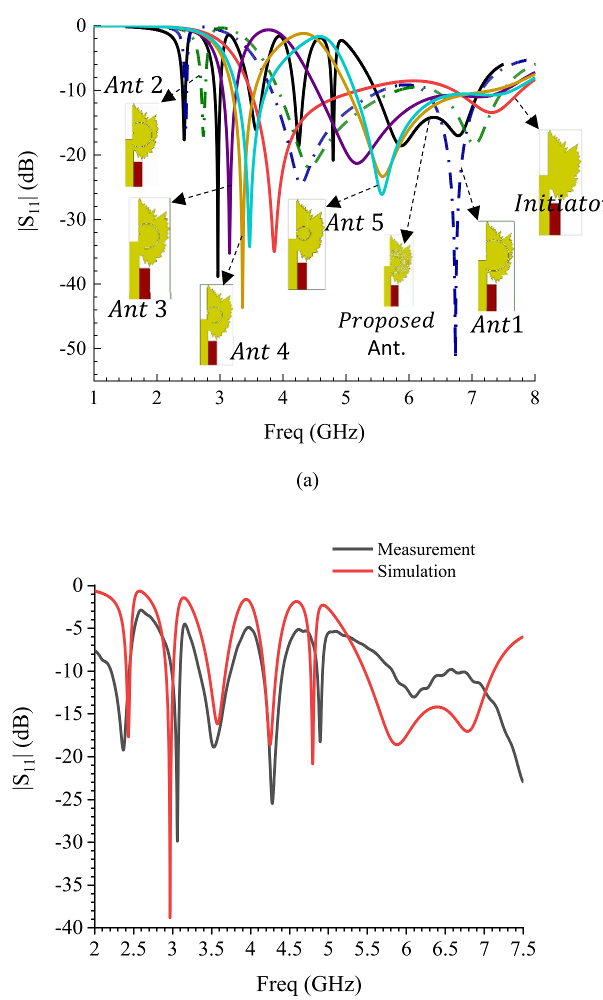

(a)

(b)

Figure 4. (a) simulated S11 of the proposed antenna evolution. (b) measured and simulated S11 of the proposed structure.

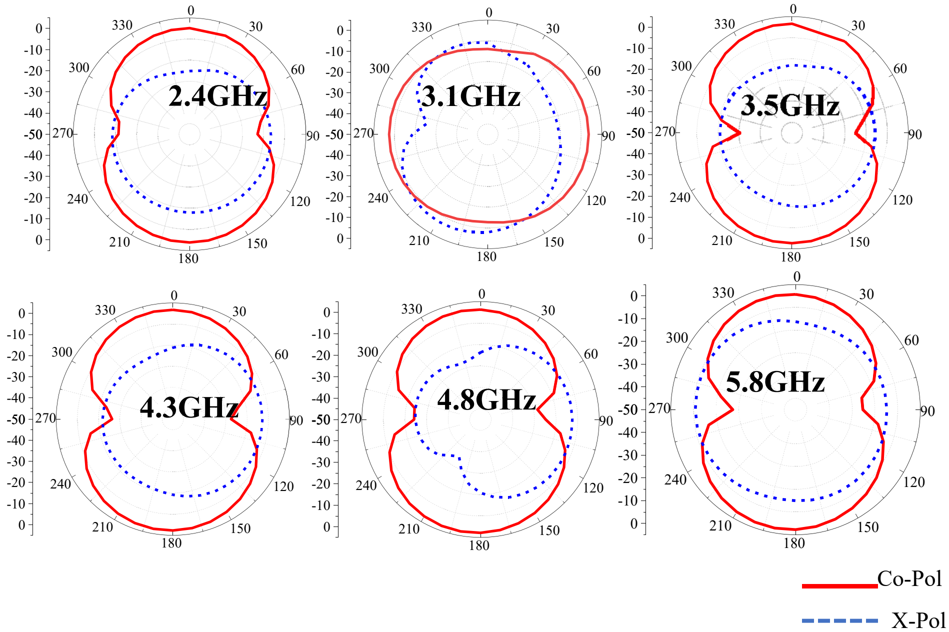

Figure 5. The simulated Radiation Pattern at XZ-plane.

the measured S11 results show that the proposed structure resonates at 2.37GHz, 3.06GHz, 3.52GHz, 4.28GHz, 4.88GHz, and 6.0GHz with a -10dB fractional bandwidth of 11.97%, 4.61%, 12.43%, 6.77%, 2.46%, and 11.55% respectively.

3.2. Antenna gain, radiation efficiency and radiation pattern

Figures 5, 6, and 7 show the radiation pattern in the XZ, YZ and XY plane respectively. It can be observed that the proposed antenna has a bi-directional radiation pattern on the XZ-plane (E-plane) while the radiation pattern in the YZ-plane (H-plane) is Omnidirectional in all its operating frequencies. In the XY-plane, it can be observed that the radiation pattern is bi-directional with a tilt as compared with the XZ-plane. The plot of the Co-Pol and X-pol radiation pattern of the proposed antenna presented in Figures 5, 6, and 7 shows that the proposed structure demonstrates a good X-pol purity in all the plane.

The Gain and Efficiency of the proposed antenna are presented in Fig. 8a and b respectively. It can be observed in Figure 8a that the gain of

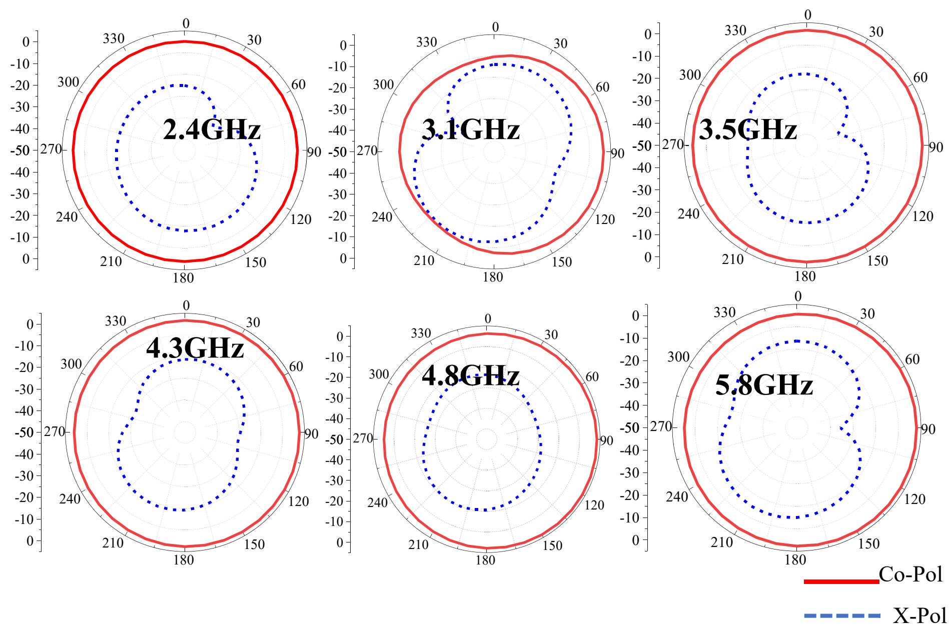

Figure 6. The Simulated Radiation pattern at YZ-plane.

$$Z_{in}=\frac{\left(R_1+j\omega L_1+\frac{1}{j\omega C_1}\right)\left(R_2+j\omega L_2+\frac{1}{j\omega C_2}\right)\left(R_3+j\omega L_3+\frac{1}{j\omega C_3}\right)\left(R_4+j\omega L_4+\frac{1}{j\omega C_4}\right)\left(R_5+j\omega L_5+\frac{1}{j\omega C_5}\right)\left(\frac{j\omega L_6R_6}{R_6\left(1-\omega^2L_6C_6\right)+j\omega L_6}+\frac{j\omega L_7R_7}{R_7\left(1-\omega^2L_7C_7\right)+j\omega L_7}\right)}{\left[\begin{array}{l}\left(\left(R_2+j\omega L_2+\frac{1}{j\omega C_2}\right)\left(R_3+j\omega L_3+\frac{1}{j\omega C_3}\right)\left(R_4+j\omega L_4+\frac{1}{j\omega C_4}\right)\left(R_5+j\omega L_5+\frac{1}{j\omega C_5}\right)\left(\frac{j\omega L_6R_6}{R_6\left(1-\omega^2L_6C_6\right)+j\omega L_6}+\frac{j\omega L_7R_7}{R_7\left(1-\omega^2L_7C_7\right)+j\omega L_7}\right)\right)+\\ \left(\left(R_1+j\omega L_1+\frac{1}{j\omega C_1}\right)\left(R_3+j\omega L_3+\frac{1}{j\omega C_3}\right)\left(R_4+j\omega L_4+\frac{1}{j\omega C_4}\right)\left(R_5+j\omega L_5+\frac{1}{j\omega C_5}\right)\left(\frac{j\omega L_6R_6}{R_6\left(1-\omega^2L_6C_6\right)+j\omega L_6}+\frac{j\omega L_7R_7}{R_7\left(1-\omega^2L_7C_7\right)+j\omega L_7}\right)\right)+\\ \left(\left(R_1+j\omega L_1+\frac{1}{j\omega C_1}\right)\left(R_2+j\omega L_2+\frac{1}{j\omega C_2}\right)\left(R_4+j\omega L_4+\frac{1}{j\omega C_4}\right)\left(R_5+j\omega L_5+\frac{1}{j\omega C_5}\right)\left(\frac{j\omega L_6R_6}{R_6\left(1-\omega^2L_6C_6\right)+j\omega L_6}+\frac{j\omega L_7R_7}{R_7\left(1-\omega^2L_7C_7\right)+j\omega L_7}\right)\right)+\\ \left(\left(R_1+j\omega L_1+\frac{1}{j\omega C_1}\right)\left(R_2+j\omega L_2+\frac{1}{j\omega C_2}\right)\left(R_3+j\omega L_3+\frac{1}{j\omega C_3}\right)\left(R_5+j\omega L_5+\frac{1}{j\omega C_5}\right)\left(\frac{j\omega L_6R_6}{R_6\left(1-\omega^2L_6C_6\right)+j\omega L_6}+\frac{j\omega L_7R_7}{R_7\left(1-\omega^2L_7C_7\right)+j\omega L_7}\right)\right)+\\ \left(\left(R_1+j\omega L_1+\frac{1}{j\omega C_1}\right)\left(R_2+j\omega L_2+\frac{1}{j\omega C_2}\right)\left(R_3+j\omega L_3+\frac{1}{j\omega C_3}\right)\left(R_4+j\omega L_4+\frac{1}{j\omega C_4}\right)\left(\frac{j\omega L_6R_6}{R_6\left(1-\omega^2L_6C_6\right)+j\omega L_6}+\frac{j\omega L_7R_7}{R_7\left(1-\omega^2L_7C_7\right)+j\omega L_7}\right)\right)+\\ \left(\left(R_1+j\omega L_1+\frac{1}{j\omega C_1}\right)\left(R_2+j\omega L_2+\frac{1}{j\omega C_2}\right)\left(R_3+j\omega L_3+\frac{1}{j\omega C_3}\right)\left(R_4+j\omega L_4+\frac{1}{j\omega C_4}\right)\left(R_5+j\omega L_5+\frac{1}{j\omega C_5}\right)\right)\end{array}\right]} \tag{20}$$

the proposed antenna is suitable for wireless communication with the least being 2.3 dBi at 2.4GHz and the highest being 3.21 dBi at 4.8GHz. The radiation efficiency of the proposed antenna is presented in Figure 8b. It can be observed that the proposed antenna has a very good radiation efficiency (71.04–100%) across its operating bands with the lowest being 71.04% at 3.1GHz.

3.3. The distribution of the surface current density

The radiation characteristics of an antenna can be well understood by analyzing its surface current distribution. Current distribution determines the electrical length (L_e) of the antenna at a specific resonant frequency using Eq. (12). The surface current distribution of the proposed antenna is presented in Figure 9.

$$f_r=\frac{C}{2L_e\sqrt{\varepsilon_{reff}}} \tag{12}$$

In the case of 2.4GHz, it can be observed that the current concentrates around the edge of the patch and the arc-slot S_1. It shows that the arc-slot S_1 contributes to the resonance at 2.4GHz as predicted in section II.

More so, at 3.1GHz, Figure 9 shows that, current concentrate on the strip formed by arc-slots S_1 and S_2. This shows that the strip formed by the combination of the two slots S_1 and S_2 is the major contributor to the resonance at 3.1GHz. It is worthy of note that though the band notch introduced by the arc-slot S_2 is maintained, there is a shift in the resonance frequency of a lone arc-slot S_2 from 2.74GHz to 3.1GHz in the combined structure. This is due to the contribution of the arc-slot S_1 as shown in Figure 9.

Furthermore, at 3.52GHz, it can be seen in Figure 9 that the major contributor is the strip formed by the arc-slots S_2 and S_3. The current distribution is seen to be concentrated on the strip between S_3 and S_4 at 4.3GHz as observed in Figure 9. This implies that the major contributor to the resonance at 4.3GHz is the strip formed by S_3 and S_4.

In the same light, the current distribution at 4.8GHz is seen to be concentrated in strip between the arc-slots S_4 and S_5. Finally, the resonance at 5.8GHz shown in Figure 9, is due to the edge around the tip of S_5.

4. Equivalent circuit design and analysis

It is a common knowledge that the antenna works with other devices in the backend such as filter, transmitter or receiver and so on. Therefore, for time domain analysis and to give the system designers insight into the EM operation of the proposed antenna, it is necessary to design its equivalent circuit. It is also a common knowledge that slotted antenna can be represented with Series-parallel combination of Resistor (R), Inductor (L) and Capacitor (C). When the slot is etched on the antenna structure, the equivalent circuit will be a combination of a series RLC in parallel to the antenna impedance which is usually denoted by a parallel RLC. With this in mind, the equivalent circuit of the proposed antenna is expected to have five (5) branches of series RLC because it has five (5)

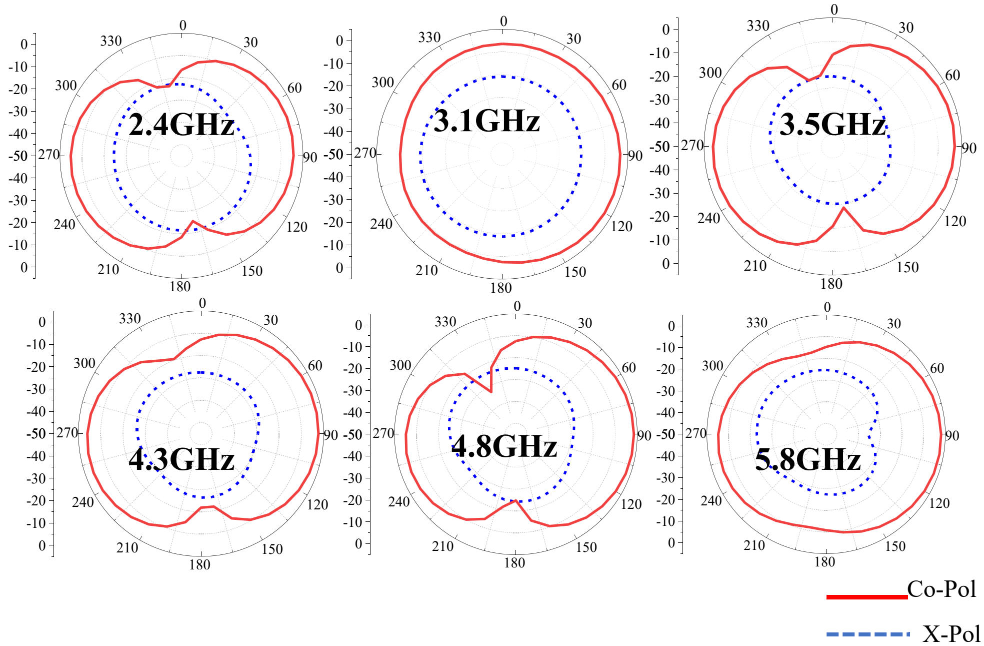

Figure 7. The Simulated Radiation pattern at XY-plane.

slots. The equivalent circuit of the proposed antenna is as shown in Figure 10. The equivalent impedance (Z_{in}) becomes,

$$\frac{1}{Z_{in}} = \frac{1}{Z_{2.74GHz}} + \frac{1}{Z_{3.03GHz}} + \frac{1}{Z_{3.88GHz}} + \frac{1}{Z_{4.49GHz}} + \frac{1}{Z_{4.71GHz}} + \frac{1}{Z_A} \tag{13}$$

where;

$$Z_{2.74GHz} = R_1 + j\omega L_1 + \frac{1}{j\omega C_1} \tag{14}$$

$$Z_{3.03GHz} = R_2 + j\omega L_2 + \frac{1}{j\omega C_2} \tag{15}$$

$$Z_{3.88GHz} = R_3 + j\omega L_3 + \frac{1}{j\omega C_3} \tag{16}$$

$$Z_{4.49GHz} = R_4 + j\omega L_4 + \frac{1}{j\omega C_4} \tag{17}$$

$$Z_{4.71GHz} = R_5 + j\omega L_5 + \frac{1}{j\omega C_5} \tag{18}$$

$$Z_A = \frac{j\omega L_6 R_6}{R_6(1 - \omega^2 L_6 C_6) + j\omega L_6} + \frac{j\omega L_7 R_7}{R_7(1 - \omega^2 L_7 C_7) + j\omega L_7} \tag{19}$$

The equivalent circuit is designed, simulated and optimized in microwave studio. The optimized value of the lump parameters is as given in Table 4. The reflection coefficient of the circuit model, EM model and measurement are presented in Figure 11. It can be observed that there is

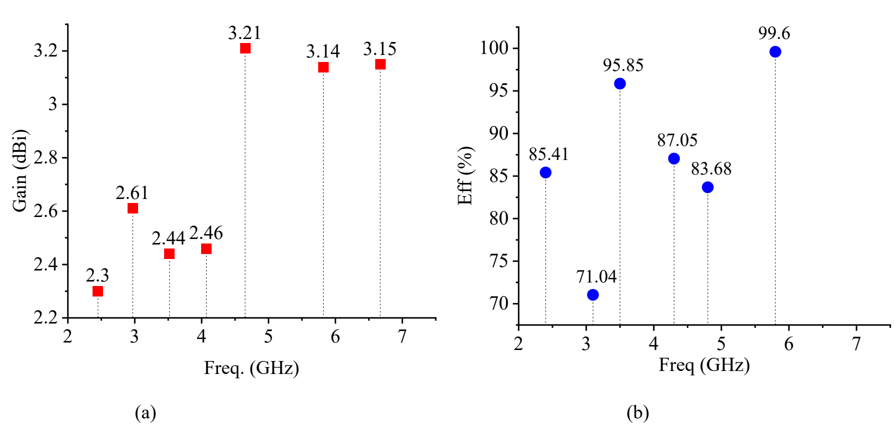

Figure 8. (a) the Gain of the proposed antenna (b) The efficiency of the proposed antenna.

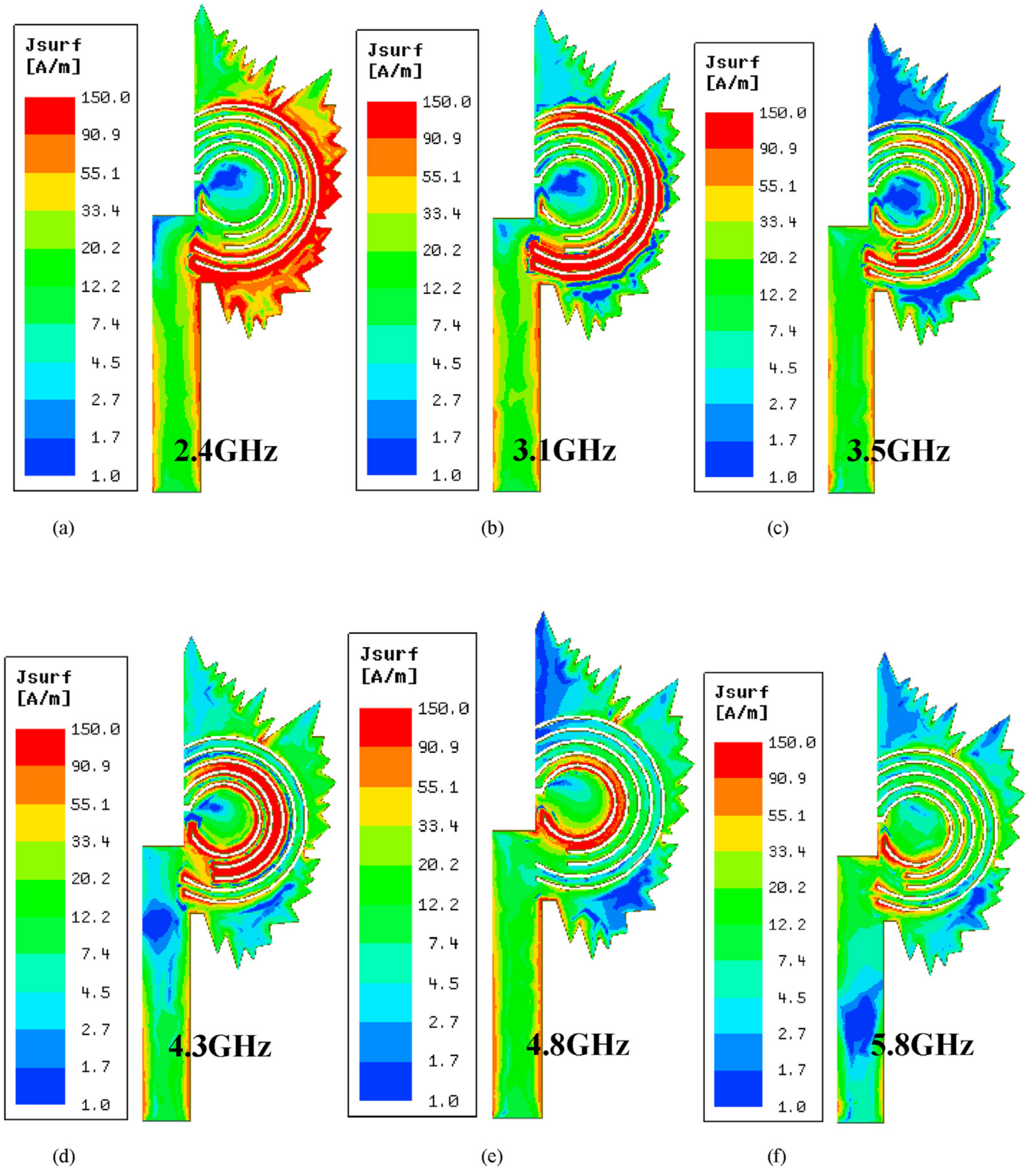

Figure 9. Surface Current Distribution of the proposed Antenna.

no significant difference among the S_{11} of the circuit model, EM model and measurement.

5. Comparative analysis

In this section, a comparative study of the proposed antenna evolution is first presented. Then, the proposed BioAs-MPA is compared with the existing works in the literature.

5.1. Comparative analysis of the proposed antenna evolution

The applications of each of the proposed antenna evolution are presented in this section. Table 5 gives the number of band and applications of each of the evolutions. It can be observed that all the antenna produced at each evolution can be used in different applications. Therefore, it can be concluded that seven different antennas (4 dual-band, 2 Tri-band, and 1 Hexa-band) are herein presented.

Table 4. The optimized value of the circuit model of the proposed antenna.

Parameters	$R1(\Omega)$	$R2(\Omega)$	$R3(\Omega)$	$R4(\Omega)$	$R5(\Omega)$	$R6(\Omega)$	$R7(\Omega)$
Value	2.5	8	7.1	18.01	32	63.5	58.3
Parameters	$L1\ (nH)$	$L2\ (nH)$	$L\ 3(nH)$	$L4\ (nH)$	$L5\ (nH)$	$L6\ (nH)$	$L7\ (nH)$
Value	304	831	44.2	54	141	0.439	0.278
Parameters	$C1\ (pF)$	$C2\ (pF)$	$C3\ (pF)$	$C4\ (pF)$	$C5\ (pF)$	$C6\ (pF)$	$C7\ (pF)$
Value	0.0139	0.00347	0.0446	0.028	0.00813	2.132	1.781

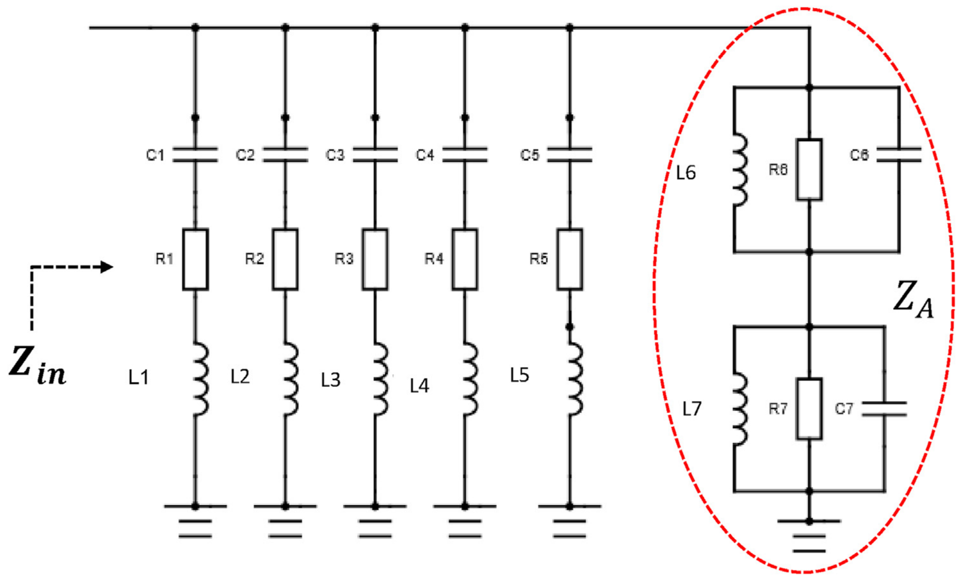

Figure 10. Equivalent circuit of the proposed antenna.

Table 5. The comparative analysis of the proposed antenna evolution.

S/N	Evolution	Frequencies (GHz)	Bandwidth (%)	Number of bands (Applications)
1	Initiator	3.86/7.32	44.8/14.7	**Dual-Band** (WiMAX, Military)
2	Ant. 1	2.46/4.3/6.74	1.2/40.9/13.8	**Tri-Band** (ISM, Radar, 5G)
3	Ant. 2	2.74/4.4/7.1	2.2/43.0/15.7	**Tri-band** (Radar, Altimeter, 5G)
4	Ant. 3	3.15/5.2	6.7/57.3	**Dual-band** (Radar, WLAN)
5	Ant. 4	3.36/5.6	11.0/41.0	**Dual-band** (5G, WLAN)
6	Ant. 5	3.47/5.58	13.8/45.1	**Dual-band** (WLAN, WiMAX)
7	**Proposed Ant.**	2.4/3.1/3.52/4.3/4.8/5.8	11.97/4.61/12.43/6.77/2.46/11.55	**Hexa-band** (ISM, LTE, radar, WiMAX, 5G, WLAN, Wi-Fi)

5.2. Comparative analysis of the proposed antennas with recent works in the literature

In order to validate the results herein presented, a comparative study with the existing works in the literature is presented in Table 6. The guided wavelength in the substrate at the lowest resonant frequency (λ_d) has been used to parameterize the size.

It can be observed in Table 6 that our work is the most compact antenna and also the highest number of bands. As far as we know, this is the only work that has presented a compact antenna with the highest number

Table 6. Comparative analysis of the BioAs-MPA antenna with recent works in the literature.

REF	SIZE (λ_d^2)	FREQ (GHz)	Bandwidth (MHz)	GAIN	EFF (%)
[25]	0.46 × 0.23	2.1/3.5/4.9	180/450/4000	*5.4 dBi	*86%
[26]	0.54 × 0.46	1.9/5.2/9.0	910/1280/2050	NR	NR
[27]	0.29 × 0.29	2/2.9/6	200/400/3400	NR	NR
[28]	0.44 × 0.49	1.22/1.57/2.45/3.42	26/90/932/172	1.75/3/6/3 (dBi)	73/63/86/57
[29]	0.31 × 0.14	2.5/3.35/5.7	280/110/550	1.7/1.5/2.05	81.1/79.6/81.5
[30]	0.35 × 0.35	3.3/5.01/7.46/9.48	NR	0.4/0.28/4.19/2.05	46.6/50.8/72.2/50.9
[5]	0.64 × 0.73	1.7/2.4	40/50	23.8 (dBm)	NR
[31]	0.49 × 0.35	2.4/3.5/5.2	120/340/1450	0.6/1.8/3.7 (dBi)	NR
[7]	0.35 × 0.76	2.4/3.5/5.5	620/1700/920	2.15/2/1.08 (dB)	NR
[10]	0.44 × 0.57	3.2/3.6/4.8	90/80/470	4.63/3.45/7.15 (dB)	NR
[15]	0.38 × 0.42	2.48/3.49	340/390	2.4/3.5 (dB)	NR
[16]	0.50 × 0.52	2.4/3.5	200/390	2.25/0.88 (dBi)	76/85
[18]	0.49 × 0.38	2.49/4.2/7.4	300/1000/800	2.92/4.13/5.85 (dB)	76.96/67.92/85.61
[21]	0.58 × 0.32	2.47/3.2/4.92	650/1450/2450	-2.25/0.56/3.25 (dBi)	NR
[20]	0.66 × 0.34	2.45/3.5/5.5	390/1080/1230	2.71/3.15/3.06 (dBi)	70/65/77
[32]	0.86 × 0.86	2.45/3.42/5.13	200/600/2330	3.29/3.37/4.16 (dB)	NR
This work	0.35 × 0.14	2.37/3.1/3.52/4.3/4.8/5.8	280/140/440/290/120/710	2.3/2.61/2.44/2.46/3.21/3.14/3.15 (dBi)	85.4/71/95.9/87.1/83.7/99.6

NR-not reported.
[*] peak value.

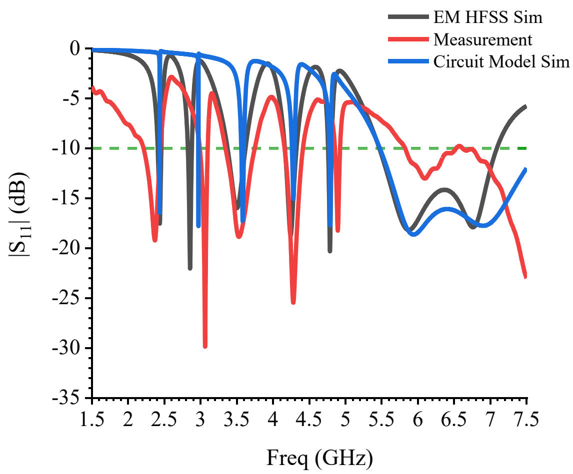

Figure 11. Reflection coefficient of the circuit model, EM model and measurement.

of narrow multiband in the open literature which is one of the contributions of this work to the existing body of knowledge.

6. Conclusion

In this paper, a bio-inspired radiating patch fed with an asymmetric microstrip line and slitting techniques have been exploited to achieve a compact Hexa-band antenna. The slits are arc-shaped which are embedded on the radiating patch. One advantage of our proposed asymmetric microstrip feeding technique is its suitability for robust antenna configuration while ensuring compactness as demonstrated in this work. The proposed antenna is suitable for Industrial, Scientific and Medical (ISM) Band, Radar, WiMAX, 5G mid-band, Bluetooth, WLAN, WiMAX, LTE, and Wi-Fi.

Declarations

Author contribution statement

Jeremiah O. ABOLADE: Conceived and designed the experiments; Performed the experiments; Analyzed and interpreted the data; Contributed reagents, materials, analysis tools or data; Wrote the paper.

Dominic B. O. KONDITI: Conceived and designed the experiments; Analyzed and interpreted the data; Contributed reagents, materials, analysis tools or data; Wrote the paper.

Vasant. M. DHARMADHIKARY: Analyzed and interpreted the data; Contributed reagents, materials, analysis tools or data; Wrote the paper.

Funding statement

This research did not receive any specific grant from funding agencies in the public, commercial, or not-for-profit sectors.

Data availability statement

Data included in article/supp. material/referenced in article.

Declaration of interests statement

The authors declare no conflict of interest.

Additional information

No additional information is available for this paper.

Acknowledgements

This work was sponsored and supported by the African Union through the Pan African University Institute of Basic Sciences, Technology, and Innovation.

References

[1] S. Su, C. Lee, S. Chen, Very-low-profile, triband, two-antenna system for WLAN notebook computers, IEEE Antenn. Wireless Propag. Lett. 17 (9) (2018) 1626–1629.
[2] S. Su, B. Tseng, Small-sized, printed 2.4/5-GHz WLAN notebook antenna aimed for 4×4 multiple transmit/receive antennas in future Gbps communications,, in: 2018 IEEE International Symposium on Electromagnetic Compatibility and 2018 IEEE Asia-Pacific Symposium on Electromagnetic Compatibility, EMC/APEMC), 2018, pp. 1084–1088.
[3] X. Pan, M. Li, S. Wang, Y. Zhou, C. Shen, X. Li, A compact multiband antenna based on metamaterial for WLAN/WiMAX/WAVE applications, in: 2017 Sixth Asia-Pacific Conference on Antennas and Propagation, APCAP), 2017, pp. 1–3.
[4] J.O. Abolade, O.A. Fakolujo, Quad-band microstrip patch antenna based on dual-cross slots, Int. J. Sci. Res. Eng. Dev. 2 (5) (2019) 1–5.
[5] R.G. Jangampally, V.K.R. Nalam, M.P. Avala, Corner cut inset-fed dual-band slot antenna for PCS and bluetooth/WLAN applications,, in: 2018 IEEE Indian Conference on Antennas and Propogation (InCAP), 2018, pp. 1–4.
[6] T. Liu, Y. Sun, CPW-fed compact multiband monopole antenna for WLAN/WiMAX application, in: 2019 IEEE MTT-S International Wireless Symposium, IWS), 2019, pp. 1–3.
[7] N. Tangthong, P. Moeikham, S. Akatimagool, A compact multi band CPW-Fed monopole antenna using L-shaped and straight slots, in: 2016 13th International Conference on Electrical Engineering/Electronics, Computer, Telecommunications and Information Technology (ECTI-CON), 2016, pp. 1–4.
[8] O.M.A. Dardeer, H. Elsadek, E.A. Abdallah, CPW-fed multiband Antenna for various wireless communications applications, in: 2018 IEEE International Symposium on Antennas and Propagation, & USNC/URSI National Radio Science Meeting, 2018, pp. 785–786.
[9] S. Singh, G. Ujjwal, M. Hashmath, S. Chilikuri, A CPW-fed monopole antenna with U-slots for triple band Application, in: 2018 9th International Conference on Computing, Communication and Networking Technologies, ICCCNT), 2018, pp. 1–6.
[10] C. Nataraj, A.A. Ismael, S. Selvaperumal, S. Khan, Compact multiband microstrip patch antenna with slot-rings for wireless applications, in: IEEE Student Conference on Research and Development: Inspiring Technology for Humanity, SCOReD 2017 - Proceedings, 2018-Janua, 2018, pp. 428–433. April.
[11] K.D. Prasad, T. Ali, R.C. Biradar, A compact slotted multiband antenna for L-band and WLAN applications,, in: 2017 2nd IEEE International Conference on Recent Trends in Electronics, Information & Communication Technology (RTEICT), 2017, pp. 820–823.
[12] R. Pandey, D.K. Vishwakarma, A meander line uniplanar EBG based multiband antenna using defected ground plane for WLAN and WiMAX applications, in: 2015 IEEE MTT-S International Microwave and RF Conference, IMaRC), 2015, pp. 64–67.
[13] A. Ghaffar, X.J. Li, B. Seet, Compact dual-band broadband microstrip antenna at 2.4 GHz and 5.2 GHz for WLAN applications, in: 2018 IEEE Asia-Pacific Conference on Antennas and Propagation, APCAP), 2018, pp. 198–199.
[14] A. Yadav, S. Goyal, T. Agrawal, R.P. Yadav, Multiband antenna for Bluetooth/ZigBee/Wi-Fi/WiMAX/WLAN/X-band applications: partial ground with periodic structures and EBG, in: 2016 International Conference on Recent Advances and Innovations in Engineering, ICRAIE), 2016, pp. 1–5.
[15] K. Kumar Naik, Asymmetric CPW-fed SRR patch antenna for WLAN/WiMAX applications, AEU - Int. J. Electron. Commun. 93 (2018) 103–108.
[16] M.M. Hasan, M. Rahman, M.R.I. Faruque, M.T. Islam, M.U. Khandaker, Electrically compact srr-loaded metamaterial inspired quad band antenna for bluetooth/wifi/wlan/wimax system, Electron 8 (2019) 7.
[17] D. Mandal, S.S. Pattnaik, Wide CPW-fed multiband wearable monopole antenna with extended grounds for GSM/WLAN/WiMAX applications, Int. J. Antenn. Propag. 2019 (2019).
[18] A.W. Mohammad Saadh, R. Poonkuzhali, A compact CPW fed multiband antenna for WLAN/INSAT/WPAN applications, AEU - Int. J. Electron. Commun. 109 (2019) 128–135.
[19] R.C. Prasad, K.D. Ali, T. Biradar, A compact slotted multiband Antenna for L-band and WLAN applications, in: 2017 2nd IEEE International Conference on Recent Trends in Electronics, Information & Communication Technology (RTEICT), 2017, pp. 820–823.
[20] C. Sim, C. Yeh, H. Lin, Compact size triple-band monopole antenna with parasitic element for WLAN/WiMAX applications, in: 2014 International Symposium on Antennas and Propagation Conference Proceedings, 2014, pp. 469–470.
[21] A.Z. Manouare, A. El Idrissi, A. Ghammaz, S. Ibnyaich, Broadband triple-band CPW-fed patch antenna for WLAN/WiMAX operations, in: 2015 International Conference on Wireless Networks and Mobile Communications, WINCOM), 2015, pp. 1–5.
[22] R.V.S.R. Krishna, R. Kumar, A slotted UWB monopole antenna with single port and double ports for dual polarization, Eng. Sci. Technol. Int. J. 19 (1) (2016) 470–484.
[23] O. Haraz, A.-R. Sebak, UWB antennas for wireless applications, in: Advancement in Microstrip Antennas with Recent Applications, 2013.
[24] I. Bahl, P. Bhartia, Microwave Solid State Circuit Design, Wiley, 2003.

[25] A. Ghaffar, X.J. Li, W.A. Awan, N. Hussain, A compact multiband multi-mode frequency reconfigurable antenna for portable devices, in: 2020 International Conference on UK-China Emerging Technologies, UCET), 2020, pp. 1–4.

[26] S. Subramanian, B. Sundarambal, Compact micro strip fed koch fractal monopole loop antenna for multiband performance, in: 2020 6th International Conference on Advanced Computing and Communication Systems, ICACCS), 2020, pp. 1438–1439.

[27] S. Dubal, A. Chaudhari, Multiband reconfigurable antenna for wireless applications, in: 2020 International Conference on Communication and Signal Processing, ICCSP), 2020, pp. 1548–1552.

[28] B.B.Q. Elias, P.J. Soh, A.A. Al-Hadi, R. Joshi, Y. Li, S.K. Podilchak, Design of a quad band CPW-fed compact flexible patch antenna for wearable applications, in: 2020 14th European Conference on Antennas and Propagation, EuCAP), 2020, pp. 1–5.

[29] J. Kulkarni, C.-Y.-D. Sim, Low-profile, compact multi-band monopole antenna for futuristic wireless applications, in: 2020 IEEE International Conference on Electronics, Computing and Communication Technologies, CONECCT), 2020, pp. 1–5.

[30] Y.V.B. Reddy, A.M. Prasad, K. V Swamy, Metamaterial inspired compact penta-band Antenna for wi-MAX, WLAN, satellite band and X-band Applications, in: *2020* IEEE International Conference on Electronics, Computing and Communication Technologies, CONECCT), 2020, pp. 1–6.

[31] H. Chen, X. Yang, Y.Z. Yin, S.T. Fan, J.J. Wu, Triband planar monopole antenna with compact radiator for WLAN/WiMAX applications, IEEE Antenn. Wireless Propag. Lett. 12 (2013) 1440–1443.

[32] A. Sharma, R.K. Gangwar, Triple band two-segment cylindrical dielectric resonator antenna with a novel microstrip feed for WLAN/WIMAX applications, Microw. Opt. Technol. Lett. 57 (11) (Nov. 2015) 2649–2655.